Knowledge-Based Systems 227 (2021) 107165

Contents lists available at ScienceDirect

Knowledge-Based Systems

journal homepage: www.elsevier.com/locate/knosys

Metric learning for novel motion rejection in high-density myoelectric pattern recognition

Le Wu [a,b], Xu Zhang [b], Xuan Zhang [b], Xiang Chen [b], Xun Chen [a,b,*]

[a] Department of Neurosurgery, The First Affiliated Hospital of USTC, Division of Life Sciences and Medicine, University of Science and Technology of China, Hefei 230001, China
[b] School of Information Science and Technology, University of Science and Technology of China, Hefei 230027, China

ARTICLE INFO

Article history:
Received 7 January 2021
Received in revised form 3 April 2021
Accepted 19 May 2021
Available online 27 May 2021

Keywords:
Human–machine interface
Myoelectric control
Novelty detection
Metric learning
Deep learning

ABSTRACT

Most traditional myoelectric pattern recognition systems can only identify limited patterns and are prone to be disturbed by unknown motion tasks. This paper is aimed to develop a robust myoelectric control method towards rejecting novel/unknown patterns. In the proposed method, we first convert high-density surface electromyogram (HD-sEMG) signals into a series of feature images. Next, a metric-learning guided convolutional neural network (CNN) is utilized to extract discriminative representations of the images. Compared to separable representations from common CNN, discriminative property characterizes representations in both the compact intra-class variations and separable inter-class differences. Subsequently, we train multiple autoencoders (AEs) to reject representations from any novel pattern that appeared significantly different from target patterns. The performance of the proposed method was evaluated using HD-sEMG signals recorded by two pieces of flexible 6×8 high-density electrode array placed over forearm extensors and flexors of nine subjects during performing seven target motion tasks and six complicated novel motion tasks. The proposed method can identify and reject novel patterns with high accuracy of 94.28%, which is significantly better than a widely adopted traditional method of 77.49% ($p < 0.05$). This work demonstrated the validity of applying metric learning in alleviating novel motion interference, which is inevitable in myoelectric control. This work will enhance the robustness of myoelectric control systems.

1. Introduction

Surface electromyography (sEMG) refers to electric signal that is collected during muscle contraction. This signal controlled by the neural system can directly reflect activation of superficial muscles, thus contains rich motor control information [1–5]. For decades, sEMG has been chosen as a command source of many human–machine interfaces (HMI) such as powered prostheses [1,4,5], exoskeleton robots [6,7], and wearable devices [8,9]. Especially, these days, the technology of myoelectric pattern recognition (MPR) enables dexterous control of multiple degrees of freedom, bringing new vigor and vitality into the field of myoelectric control. The MPR technology aims to automatically discover regularities in sEMG signals through computer algorithms and with these regularities to interpret the motor intention. Many studies have demonstrated its effectiveness and superiority when applied to various HMIs under laboratory conditions, in which >95% of classification accuracy for >10 classes of hand and forearm motion tasks were achieved [10–15]. Among them, the combination of time-domain (TD) features [16] and linear discriminant analysis (LDA) classifier [1] has been widely adopted due to its satisfactory performance and minimal computational burden.

Although the MPR technology has been well explored in the academic community, it has not been extensively applied in commercial products. Some impediments faced when transitioning to clinical situations, such as the interference of novel motion tasks [17–25], electrode shift [14,26,27], variation in contraction strength or limb orientation [12,28,29], that may lead to performance degradation.

In this study, we are interested in alleviating the interference of the novel motion tasks. Traditional MPR based systems often constrain the data collection scenario (training session), providing a limited number of classes of motion tasks (target motion tasks). This may not represent clinical scenarios in which novel motion tasks, i.e., the tasks that are not included in the training session, may be performed and will be inevitably misclassified. Take LDA as an example; this classifier identifies each feature vector according to the Bayes rule, which picks a maximum posterior probability class. When a feature vector from any novel motion task is inputted, the classifier has to decide within all learned

* Corresponding author.
E-mail addresses: wule1994@mail.ustc.edu.cn (L. Wu), xunchen@ustc.edu.cn (X. Chen).

https://doi.org/10.1016/j.knosys.2021.107165
0950-7051/

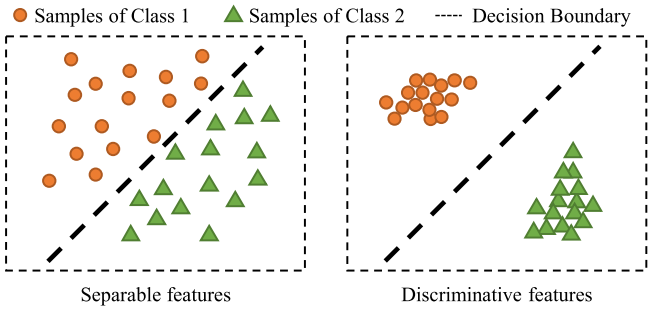

Fig. 1. Examples of separable (left) and discriminative (right) features.

patterns and thus clearly produces an error. In practice, it is impossible to force the users to conduct only the target motion tasks, and the unavoidable variability in real life makes the novel motion tasks unavoidable. As a result, frequent erroneous outputs may cause unsmooth control and provide negative feedback to users. Therefore identifying and rejecting novel motion tasks is of utmost importance.

We think that three aspects may help catch the subtle difference between target and novel tasks: sufficient information sensing, the powerful ability of signal representation, and the practical rejection approach. The first one is the easiest to think of, that is to increase the number of electrodes and enlarge the detection region so as to record sufficient motor control information for subsequent processing. Therefore, the use of high-density sEMG (HD-sEMG) is prevalent and beneficial. Compared to single-channel sEMG, it is reported that the HD-sEMG that contains additional temporal–spatial information can boost the performance of myoelectric control [10,11,14,15,30].

After the collection of HD-sEMG, the most exciting and challenging procedure is to find a proper manner to represent the signals. From our point of view, this procedure plays a key role in rejecting novel motion tasks. Different from routine classification learning, the aim of novel motion rejection is not only to classify the motion intentions, but also to reject the contractions that have different patterns. This means the extracted features/descriptions of HD-sEMG need to be both separable and discriminative. Discriminative property characterizes features in both the compact intra-class variations and separable inter-class differences. From Fig. 1, it can be observed that the discriminative features may help detect novel patterns in two ways: one is that the compacting intra-class variations could help the subsequent rejection method to model the distributions of target tasks more efficiently, and the other is that enlarging inter-class differences makes the features to be sensitive to differences in HD-sEMG patterns, implying a larger distance between novel samples and target samples [31].

This study utilizes a metric-learning guided convolutional neural network (CNN) to extract the discriminative features from HD-sEMG. Recently, many studies claim that deep learning with CNN has great advantages in mining information of HD-sEMG [14,26,32–37]. However, most of these studies only focus on the close-set classification problem; that is to say, the classes of testing samples are assumed to be within the training dataset, so although the features extracted by CNN have superior performance in terms of separability, they may not be discriminative. Therefore, we use the idea of metric learning to modify the training strategy of CNN. The goal of metric learning is to learn a function that assigns small distances to samples from the same task and relatively large distances to that from different tasks, such that the outputs of the function are regarded as the discriminative features [38]. Subsequently, with the help of these features, we select autoencoder (AE) as the rejection method, which is a popular and powerful reconstruction-based approach. We train one AE for each target task to reject samples that have high reconstruction errors. In the following chapters, we will describe all these procedures in detail.

2. Related work

There are various studies for alleviating the interference of novel tasks, which can roughly be categorized into domain-based, probability-based, and reconstruction-based approaches. The domain-based approaches aim to find a boundary to enclose the samples from target motion tasks so that the samples that fall beyond the boundary are designated to be novel. Typical studies are designing a one-class classifier using support vector data description [18,19], Mahalanobis distance [21,22], and multiple one-versus-one classifiers [17,20]. Probability-based methods attempt to assign high posterior probability estimation to target samples and low estimation to novel samples, based on the data distribution learned by classifiers. The representative works made use of the probability produced by LDA [23], support vector machine [24], and artificial neural network [25] to filter out the novel samples. These days, reconstruction-based approaches are attracting increasing attention, which utilize AEs and their variants to find compressed representations from complex data, and the novel samples can hence be rejected via their high reconstruction error [39,40].

In general, the aforementioned studies postulate that the intrinsic geometry of target and novel samples are fairly different (usually, novel motion tasks are actually known, classifiable contractions), and hence can be simply separated by modeling only the distribution of each target class. In true usage scenarios, however, the novel samples may be unpredictable and much similar to target samples. For example, when manipulating a robot, we predefine four hand and wrist motions for controlling: wrist pronation/supination, hand open/close. During the operations, the user may need to do some other meaningful activities such as recording logs with keyboard or mouse, performing handwriting tasks. Here, at some point, the use of a keyboard or mouse may involve muscular contractions similar to the wrist pronation, and the contractions from handwriting may be similar to that of hand close. Meanwhile, the prosthetic users may also suffer from the same issue when performing unconscious muscular contractions during motion transitions or changes in limb positions. It stands to reason that an intelligent HMI system should not respond to these similar but novel, unavoidable activities. Additionally, given the fact that differences among these contractions are pretty subtle, rejecting novel motion tasks in practice presents new challenges.

3. Methods

The flowchart of the proposed method is illustrated in Fig. 2, and the whole method involves three procedures. We first convert HD-sEMG data into a series of images, where the highlight regions represent activations of different muscles. Given the HD-sEMG images, it has been proven that CNN is able to extract spatial information efficiently [14]. In addition, we customize a metric learning-based CNN to extract discriminative features from the images, whereas only separable features that most routine classification tasks care about. The last procedure is to use multiple AEs to reject samples with incongruity characteristics.

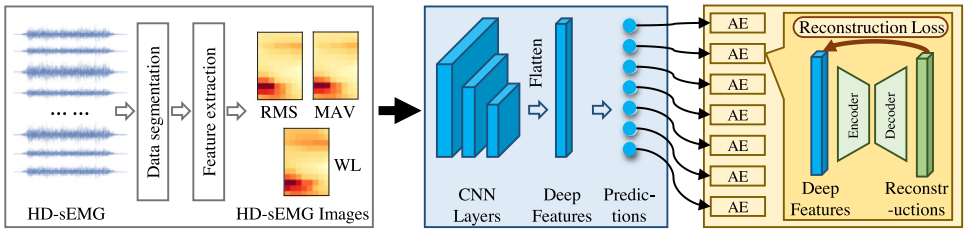

Fig. 2. An overview of the proposed method.

3.1. Procedure 1: Convert HD-sEMG into images

The contribution of this procedure is to preprocess the HD-sEMG signals into images. Specifically, we first segmented the collected multichannel sEMG signals into a series of overlapped analysis windows with a window length of 250 ms and an increment of 150 ms. Next, the windows of quiescent baseline conditions were cast off through an amplitude thresholding manner. The threshold was defined as mean plus three times the standard deviation of the previously collected quiescent signals [23]. Three time-domain (TD) features, namely root mean square (RMS), mean absolute value (MAV), and waveform length (WL), were extracted from each channel of one analysis window. Please refer to [1] for calculation details. These features have been shown to intuitively reflect muscular contractions with low computational complexity [14–17]. Our previous works also showed that the combination of TD features and a small-scale CNN could achieve satisfactory myoelectric control performance [27,33]. Finally, a feature matrix in the form of $m \times n \times 3$ was obtained from each analysis window by extracting features from all the channels of the HD electrode array, where $m \times n$ represented the integrated channel deployment of the adopted electrode array. These feature matrices were further regarded as images with the resolution of $m \times n$. Besides, we considered these images as the basic samples for subsequent procedures of model training or testing.

3.2. Procedure 2: Describe HD-sEMG images using CNN and metric learning

This procedure is to extract discriminative features from the HD-sEMG images. As shown in Fig. 3, a multi-layer CNN architecture that included two convolutional layers, one flatten layer, and two fully-connected layers are adopted (the detailed configurations were illustrated in the figure). It is worth noting here that the discriminative property of the deep features (the outputs of the layer 4) extracted by this network is guaranteed by the use of softmax loss and center loss functions, synchronously; whereas many previous studies have trained CNN only with the softmax loss:

$$\mathcal{L}_S = -\frac{1}{N}\sum_{i=1}^{N} log\frac{e^{\boldsymbol{w}_{y_i}^T \boldsymbol{x}_i + b_{y_i}}}{\sum_{k=1}^{K} e^{\boldsymbol{w}_k^T \boldsymbol{x}_i + b_k}} \tag{1}$$

where $\boldsymbol{x}_i \in \mathbb{R}^d$ and y_i are the deep feature and label of the ith sample, respectively. $\boldsymbol{w}_k \in \mathbb{R}^d$ is the kth column of the parameters $\boldsymbol{W} = [\boldsymbol{w}_1, \boldsymbol{w}_2, \ldots, \boldsymbol{w}_K] \in \mathbb{R}^{d \times K}$, which connected deep features to the final layer. $\boldsymbol{b} \in \mathbb{R}^K$ is the bias. N, K and d represent the number of mini-batch samples, the number of task categories and dimensions of deep features, respectively.

The softmax activation (the content within the $log(\cdot)$ function in Eq. (1) is equivalent to applying a linear operator defined by $\boldsymbol{W}$ and $\boldsymbol{b}$ to the $\boldsymbol{x}$, thus mapping the highly-dimensional deep features to different categories. Further, the softmax loss will be minimized if all samples were classified properly, indicating that the lower the softmax loss, the better separability of the deep features is achieved.

Fig. 4 demonstrates the distributions of deep features produced only by the softmax loss function, using a visualization technique of t-distributed stochastic neighbor embedding (t-SNE) [41]. It is worth noting that although the features are likely to be separable in a highly-dimensional space, they may not be clustered well and are prone to be overlapped in certain regions, resulting in weakly discriminative power and difficulties in subsequent novel motion rejection.

Inspired by Wen et al. [38], we took use of the knowledge of metric learning to learn discriminative features by CNN. Specifically, in addition to the softmax loss function, a center loss is implemented to train the network jointly. The center loss can be formulated as:

$$\mathcal{L}_C = \frac{1}{2N}\sum_{i=1}^{N} D\left(\boldsymbol{x}_i, \boldsymbol{c}_{y_i}\right) \tag{2}$$

here, $\boldsymbol{c}_{y_i} \in \mathbb{R}^d$ was the center of the class y_i. $D(\cdot)$ measures the squared Euclidean distance between two elements. During training, the parameter centers $\boldsymbol{C} = [\boldsymbol{c}_1, \boldsymbol{c}_2, \ldots, \boldsymbol{c}_K] \in \mathbb{R}^{d \times K}$ are updated using mini-batch samples at each iteration. Therefore, this loss function penalizes distances between deeply learned features and their centers, thus pushing instances of the same category towards the center of the category.

Finally, combined with the softmax loss, the joint supervision loss function can be written below:

$$\mathcal{L}_{total} = \mathcal{L}_S + \lambda\mathcal{L}_C = -\frac{1}{N}\sum_{i=1}^{N} log\frac{e^{\boldsymbol{w}_{y_i}^T \boldsymbol{x}_i + b_{y_i}}}{\sum_{k=1}^{K} e^{\boldsymbol{w}_k^T \boldsymbol{x}_i + b_k}} + \frac{\lambda}{2N}\sum_{i=1}^{N} D\left(\boldsymbol{x}_i, \boldsymbol{c}_{y_i}\right) \tag{3}$$

where hyper-parameter λ controls the trade-off between the center loss and softmax loss. Intuitively, this combination maximizes inter-class distance using the softmax loss function while minimizing intra-class distance with the center loss function. Besides, since the process of random initialization and mini-batch-based updating of centers $\boldsymbol{C}$ may be tricky and unstable, the softmax loss with clear supervisory information could guide $\boldsymbol{C}$ to converge into better class centers [38]. Fig. 5 reveals the influence of λ on feature distributions. The distributions of deep features appears to be discriminative with proper λ, which is crucial for novel motion rejection.

In order to train the network, the AdaDelta algorithm [42] is adopted with the batch size set to 16. We optimized the network using the training samples for 50 epochs with a learning rate of 0.1 and fine-tuned it with a learning rate of 0.01 for another 50 epochs. The trained CNN is used for extracting discriminant features, and the parameters are fixed during training the subsequent AEs.

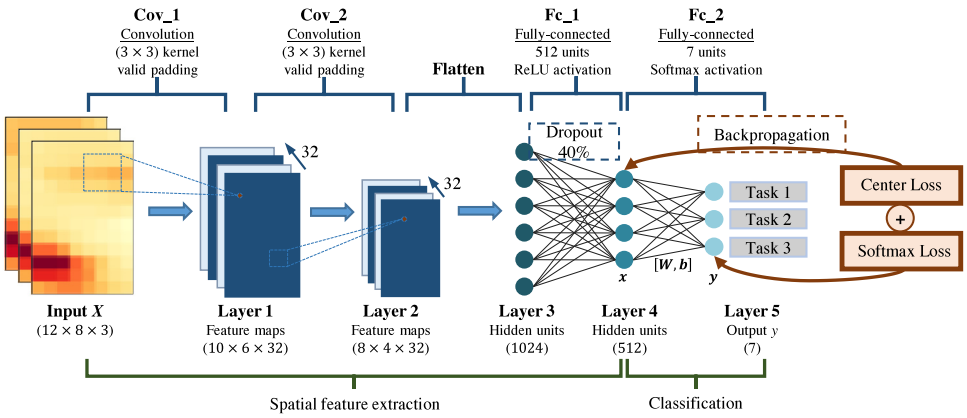

Fig. 3. The architecture of the CNN adopted in this study. This CNN consists of 5 layers, including two convolutional layers, one flatten layer and two fully-connected layers. During training, the dropout rate between Fc_1 and Fc_2 is set to 40%. A joint loss function, i.e. center loss and softmax loss, is applied to optimize the network.

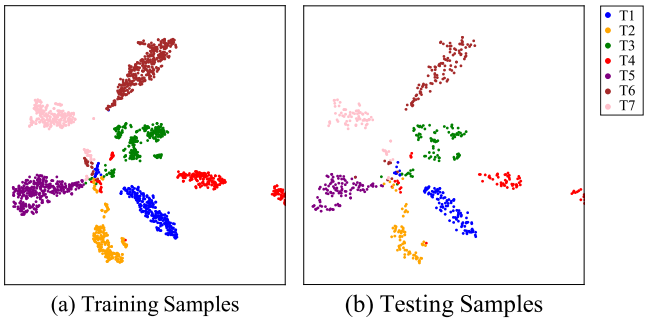

Fig. 4. Visualization of deep features trained without center loss. The features are extracted from training samples (a) and testing samples (b) of subject 1. The scattered points represent samples, with colors to indicate different patterns.

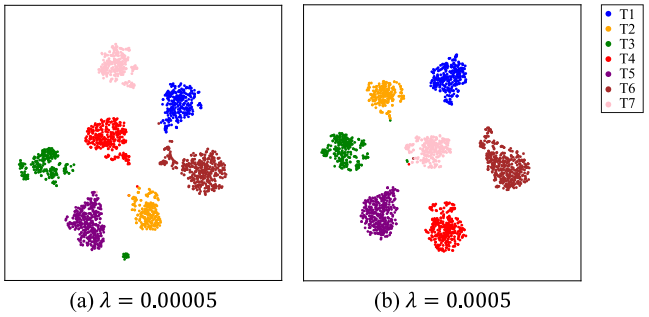

Fig. 5. Visualization of deep features trained with center loss. λ denotes the weight of center loss. The samples are from subject 1. The scattered points represent samples, with colors to indicate different patterns.

3.3. Procedure 3: Reject novel samples using AE

Given the discriminative features, the next step is to reject samples with characteristics different from those of any target patterns. As described in Fig. 2, we trained multiple AEs based on the deep features of each target pattern. The CNN obtained in procedure 2 is able to give a prediction (one of the target patterns) to any given input sample, no matter whether it is from a target or novel pattern. The role of AE is to act as a watchdog; that is, after the CNN makes a prediction, it examines whether the current input sample follows the predicted pattern's distribution. The system does not respond to any input if it is considered to come from a novel pattern.

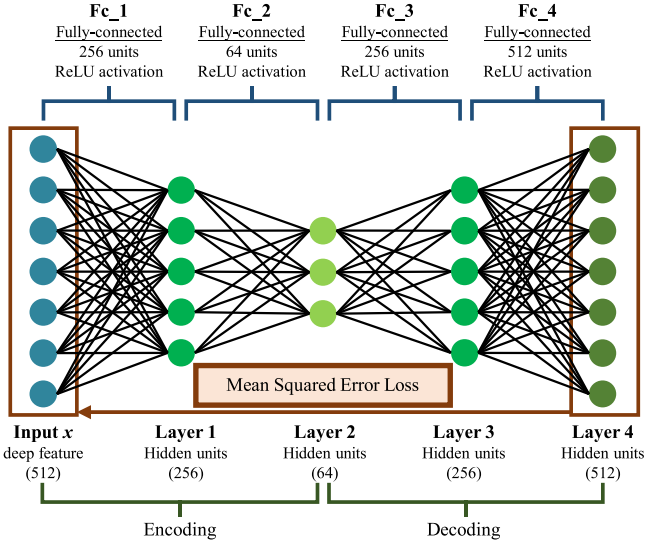

Fig. 6. The architecture of the autoencoder (AE) adopted in this study. This network consists of one input layer and four fully-connected layers.

The architecture of AE implemented in this study is described in Fig. 6. The AE consists of one input layer and four fully connected layers. During the training phase, we have deep features of one target pattern as training set $\boldsymbol{X} = [\boldsymbol{x}_1, \boldsymbol{x}_2, \ldots, \boldsymbol{x}_m] \in \mathbb{R}^{d\times m}$. m is the number of samples belonging to the target pattern. The left part (layer 1, 2) of this symmetrical network is aimed to learn a compressed representation (encoding) for a set of data, in which deep features of the target patterns and novel patterns appear to be significantly different [39], while the right part (layer 3, 4) reproduced the encodings (decoding) to their original form $\hat{\boldsymbol{X}} = [\hat{\boldsymbol{x}}_1, \hat{\boldsymbol{x}}_2, \ldots, \hat{\boldsymbol{x}}_m] \in \mathbb{R}^{d\times m}$, so that the reconstruction loss (mean square error loss) becomes small. The stochastic gradient descent (SGD) algorithm with mini-batch is adopted to optimize the parameters in the network. The number of the batch size is 16. We train the network with a learning rate of 0.1 for the first 600 epochs and fine-tune it with a learning rate of 0.01 for another 300 epochs. In summary, the two networks are trained in a sequence manner: the CNN is trained first as a feature extractor, and then the AE is trained using deep features produced by CNN while the CNN's parameters are fixed.

During the testing phase, the reconstruction error is empirically computed according to Bray Curtis distance [43]:

$$Err_i = \frac{\sum_{j=1}^{d} \left| \boldsymbol{x}_{ij} - \hat{\boldsymbol{x}}_{ij} \right|}{\sum_{j=1}^{d} \left(\boldsymbol{x}_{ij} + \hat{\boldsymbol{x}}_{ij} \right)} \tag{4}$$

where $\boldsymbol{x}_{ij}$ denotes jth element in the vector $\boldsymbol{x}_i$. This distance function has a similar effect to the function of cosine similarity that is always utilized to measure the distance between two high dimensional non-negative vectors. Finally, when a testing sample is inputted to the proposed method, a deep feature and the prediction are first produced by CNN. Then, the corresponding AE is activated to measure the difference between the current deep feature and the target distribution. The reconstruction error is expected to be very large if the current sample comes from a novel task; otherwise, the error is small. A threshold is thus necessary for each AE to reject novel samples. Actually, the determination of the threshold is a trade-off process; that is to say, a higher threshold will introduce more target and novel samples at the same time, while a lower threshold may inevitably reject some target samples. In this study, we use the reconstruction errors of the validation set to select the thresholds. Specifically, we first preset a recall (also known as sensitivity) factor on the validation set for all AEs, and then record the corresponding reconstruction value of the validation sample that exactly reaches the factor as the threshold of each AE. A high recall factor implies that more target testing samples can pass through AEs, and vice versa.

In summary, if the AE believes that the testing sample comes from a target task, the corresponding prediction of the CNN is assigned to be its label. In this study, the configurations of the aforementioned networks are determined with several pre-tests. The algorithm was developed using a deep-learning software called Keras. All programs were implemented on a laptop with an Intel i7 GPU, 16 GB RAM, and a GPU of NVIDIA GeForce GTX 1050Ti. We have also published the source codes online[1] for quick reproduction and further clarification.

3.4. Evaluation metrics

In order to fairly verify the performances of various methods, the receiver operating characteristic (ROC) curve [44] was adopted. The ROC curve illustrates the diagnostic ability of the binary classifiers for identifying novel/ target samples as the threshold varied, and a higher area under the curve (AUC) indicates that the model is better at distinguishing novel samples.

Besides, the classification accuracy of each class was also calculated after the threshold was determined, which was the ratio of the number of correct predictions to the total number of input samples.

The proposed method was conducted in a user-specific manner. For each subject, we repeated the experiments five times to get the average metrics.

3.5. Comparison methods

To evaluate the performance of the proposed method, several baseline methods have been implemented:

TD features with LDA classifier (TD + LDA) [1] first extracts time-domain features from sEMG signal windows and then identifies motion samples with the LDA classifier. This pattern-recognition method is widely adopted in the myoelectric control field due to its satisfactory performance and minimal computational burden.

TD + LDA with Mahalanobis distance (TD + LDA-MD) [21,22] improves the TD + LDA method with the novelty detection ability. We can view the LDA as replacing Procedure 2 in the proposed framework, which transformed the raw TD features into compressed feature vectors and, meanwhile, predicted categorical class labels. Similarly, the subsequent MD function measured the distance between testing samples and training dataset according to:

$$MD_i = \left(\boldsymbol{s}_i - \boldsymbol{\mu}_{y_i} \right)^T \Sigma_{y_i}^{-1} \left(\boldsymbol{s}_i - \boldsymbol{\mu}_{y_i} \right) \tag{5}$$

where $\boldsymbol{s}_i$ refers to the compressed feature vector of the ith sample. $\boldsymbol{\mu}_{y_i}$ and Σ_{y_i} are the class mean vector and covariance matrices of the training dataset of class y_i. We can reject novel classes according to relatively large distances between novel samples and target samples.

CNN with distance rejection [38]**:** we use CNN, which is trained using softmax loss and center loss, to extract deep features. The distances between centers and inputted samples' deep features are computed by the Cosine Similarity. The novel samples are rejected because of their large distances to each center. Similar to the proposed method, multiple thresholds are calculated with the validation dataset. We denote this comparison method as **CNNSC + DR**.

CNN with LDA-MD first uses CNN to extract deep features from HD-sEMG feature images and then applies the LDA-MD method to reject novel classes. According to different loss functions, two comparison methods are implemented, i.e., **CNNS + LDA-MD** and **CNNSC + LDA-MD**, where CNNS and CNNSC represent the deep features extracted from the CNN trained by the softmax loss only, and the joint supervision loss (softmax loss and center loss), respectively.

CNN with AE, same to the above method, uses CNN to extract deep features and AE to reject novel classes. Similarly, **CNNS + AE** and **CNNSC + AE** methods are implemented, where CNNSC + AE is the proposed method of this study.

It is noted that, except for the TD + LDA method (it does not need a threshold), the processes of determining rejection thresholds for all comparison methods are the same as the corresponding part of Procedure 3 in the Methods section.

3.6. Statistics

One-way ANOVAs with repeated measures were conducted to compare the AUCs and classification accuracies obtained from six methods (TD + LDA-MD, CNNSC + DR, CNNS + LDA-MD, CNNSC + LDA-MD, CNNS + AE, and CNNSC + AE). Posthoc multiple pairwise comparisons were conducted with Bonferroni corrections. The significant level was set to 0.05. We performed these analyses using SPSS software (ver. 24.0, SPSS Inc. Chicago, IL, USA).

4. Experiments and results

4.1. Experiment setup

4.1.1. Subjects

Nine able-bodied subjects were recruited in this study (six males, three females; all right-hand; aged from 22 to 27). The data collection protocol was approved by the Ethics Review Board of the University of Science and Technology of China. The experimental content was introduced to each subject in detail, following which their written consent was obtained.

[1] https://github.com/NMClib/noveltyRejection_MetricLearning.

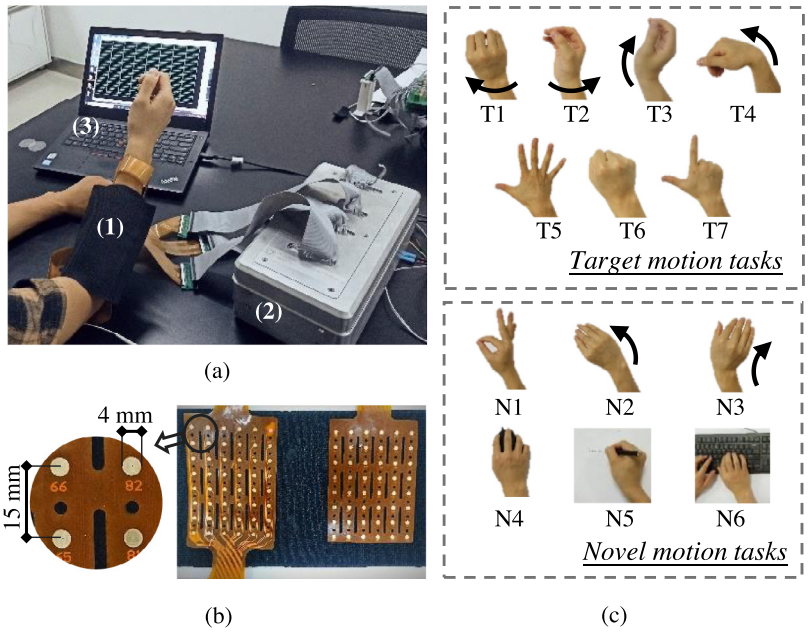

Fig. 7. Experimental devices and scenario. (a) demonstrates the experimental scenario including two high-density electrode arrays concealed in the textile (1), a customized signal recording device (2) and a software for real-time storage and display of HD-sEMG signals (3). (b) shows the configuration of the adopted electrode arrays. (c) illustrates 13 motion tasks, including 7 target tasks and 6 novel tasks.

4.1.2. Data collections

Fig. 7 illustrates the setup adopted in this study. Two pieces of flexible high-density electrode array (Fig. 7b) were designed to record HD-sEMG from forearm muscles in the dominant side of all subjects. Each array consisted of 48 monopolar sEMG channels in the form of a 6×8 matrix. The electrode diameter and distance between two consecutive electrodes were 4 mm and 15 mm, respectively. A signal recording system was also customized, which can be seen in Fig. 7a. The system first amplified and filtered the analog sEMG signal of each channel by a two-stage amplifier of 60 dB gain and a band-pass filter of 20–500 Hz. Subsequently, the signals were sampled at 1 kHz with a 16-bit analog-to-digital converter. All digitalized signals were then transmitted to a computer via a USB cable, and the corresponding recording software has also been developed.

During the experiments, the subjects were seated comfortably in a chair with their forearm limbs relaxed on a height-adjustable table. Their forearm skin was cleaned with 70% isopropyl alcohol, and two reference electrodes were attached to the olecranon of both arms. Both high-density electrode arrays were integrated into a stretchable textile to ensure high quality of skin-electrode contact. All subjects were asked to perform thirteen different motion tasks, including seven target motion tasks and six novel motion tasks, as shown in Fig. 7c. Seven target tasks were wrist pronation (T1)/supination (T2), wrist extension (T3)/flexion (T4), hand open (T5)/close (T6) and shoot (T7). The six novel tasks can be grouped into two categories. One was static novel tasks, of which previous studies usually investigated, and they were pinch (N1), radial deviation (N2), and ulnar deviation (N3). Another category was dynamic tasks that included mouse manipulating (N4), hand writing (N5) and keyboard typing (N6). The dynamic tasks were designated according to their frequent occurrences in daily life. In each collection experiment of T1–T7 and N1–N3, the experimenter instructed subjects to maintain a mild muscular contraction of the task for 10 repetitions, and each repetition lasts roughly 5 s. For each task of N4–N6, subjects were asked to perform for about one minute while the HD-sEMG signals were collected from the dominant limb. Adequate rest periods between consecutive experiments were allowed to avoid muscular and mental fatigue of the subjects. At last, we also collected a period of sEMG signals during quiescent baseline conditions, which was used for casting off no motion data.

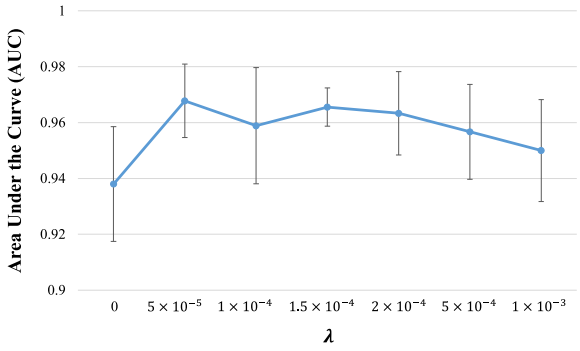

Fig. 8. AUC values of ROCs averaged over all subjects, achieved by the proposed method (CNNSC+AE) with different λ values. The CNNSC+AE method is the same as the CNNS+AE method when the λ is set to 0.

In order to facilitate the data processing, we randomly divided the samples of target motion tasks into the training, validation, and testing set, following the ratio of 64%, 16%, and 20%, respectively. The dataset used in this study is shown in Table 1.

4.2. Experiments on different hyperparameter λ

The hyperparameter λ influences the performance of the proposed method by dominating the distributions of the deep features. As shown in Fig. 8, we vary λ from 0 to 0.001 to observe the performance changes of the corresponding models. It is worth noting that the model trained only with softmax loss (λ is 0) yields the worst AUC of 0.938, while a proper λ can improve the model performances, and the improvements are stable for a large range of λ. In the following sections, we fix λ to 5×10^{-5}.

4.3. Performance of rejecting novel motion tasks

As can be seen from Fig. 9, we compute the true positive rate (TPR) and false positive rate (FPR) under different thresholds, and

Table 1
Experiments dataset used in this study.

Subject Id	Gender	Age	Training signals (7 target motion tasks)	Validation signals (7 target motion tasks)	Testing signals (7 target motion tasks + 6 novel motion tasks)
1	M	26	408.25 s	102.06 s	127.58 + 469.95 s
2	M	25	441.56 s	110.39 s	137.99 + 459.30 s
3	M	27	470.94 s	117.73 s	147.17 + 484.20 s
4	F	24	391.16 s	97.79 s	122.24 + 522.30 s
5	M	27	238.43 s	59.60 s	74.51 + 338.55 s
6	F	22	453.08 s	113.27 s	141.59 + 456.00 s
7	M	25	329.44 s	82.36 s	102.95 + 388.65 s
8	M	27	249.28 s	62.32 s	77.90 + 392.85 s
9	F	25	334.33 s	83.58 s	104.48 + 382.50 s
Avg.	n.a.	25.33 ± 1.56	368.49 ± 80.90 s	92.12 ± 20.22 s	547.85 ± 77.95 s

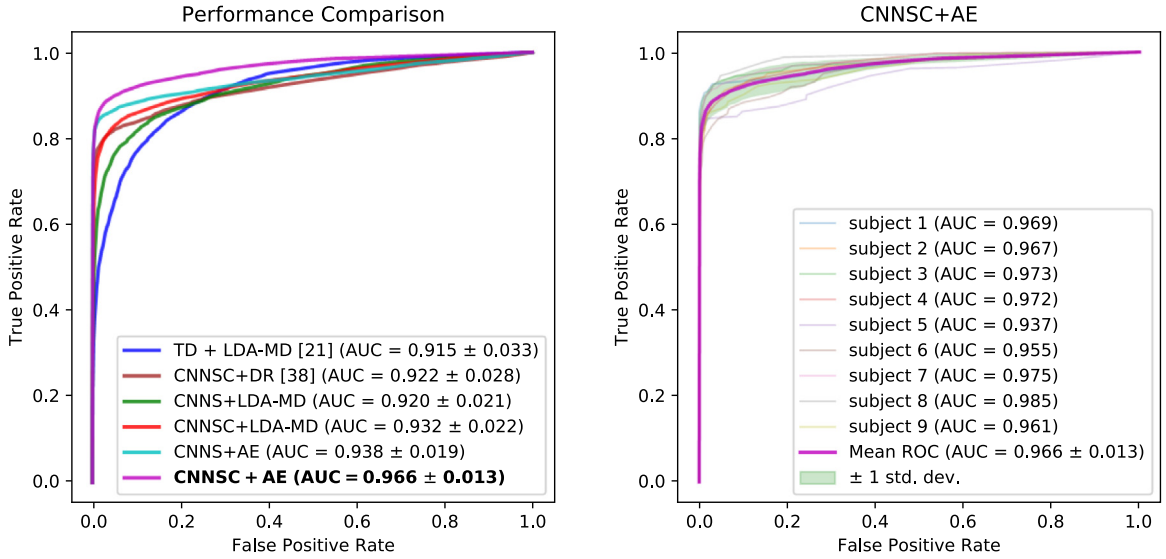

Fig. 9. (a) illustrates ROC curves averaged over all subjects of the six methods. (b) demonstrates the ROC curves of all subjects obtained by the proposed method (CNNSC + AE), in which the bold purple curve is the average curve and the green region represents the standard deviation.

Table 2
Classification accuracies (%) of target and novel motion tasks using different methods when the recall factor is set to 0.8 and 0.9, respectively. The accuracies are averaged over all subjects. The CNNSC + AE is the proposed method.

Recall factor	Method	Target motions	Novel motions						
		Avg.	Typing	Writing	Mouse manipulating	Pinch	Ulnar deviation	Radial deviation	**Avg.**
	TD + LDA [1]	**95.30 ± 2.00**	0	0	0	0	0	0	0
0.8	TD + LDA-MD [21]	78.92 ± 2.86	91.26 ± 8.65	85.74 ± 12.63	90.26 ± 9.25	75.41 ± 18.79	91.44 ± 8.49	94.26 ± 5.85	88.06 ± 12.97
	CNNSC + DR [38]	78.27 ± 2.52	94.22 ± 10.75	97.00 ± 3.83	96.11 ± 6.87	97.33 ± 4.40	94.89 ± 9.04	98.00 ± 2.62	96.26 ± 7.02
	CNNS + LDA-MD	79.18 ± 2.66	93.19 ± 7.23	90.78 ± 6.54	94.59 ± 4.86	85.07 ± 17.46	94.11 ± 5.24	95.15 ± 6.44	92.15 ± 9.70
	CNNSC + LDA-MD	78.45 ± 2.29	97.41 ± 2.37	97.30 ± 2.44	97.78 ± 2.27	94.56 ± 5.41	96.56 ± 4.84	97.41± 2.16	96.83 ± 3.68
	CNNS + AE	78.61 ± 1.97	99.33 ± 1.03	**99.81 ± 0.36**	**99.93 ± 0.21**	99.44 ± 0.83	**99.74 ± 0.62**	**99.93 ± 0.14**	**99.70 ± 0.66**
	CNNSC + AE	78.36 ± 2.58	**99.89 ± 0.22**	99.70 ± 0.48	99.67 ± 0.83	**99.56 ± 0.47**	99.56 ± 0.57	99.41 ± 0.86	99.63 ± 0.63
0.9	TD + LDA-MD [21]	88.43 ± 2.73	82.30 ± 11.72	75.52 ± 16.30	79.93 ± 11.41	53.85 ± 22.66	83.96 ± 14.44	89.37 ± 9.26	77.49 ± 18.78
	CNNSC + DR [38]	88.45 ± 2.11	69.22 ± 26.09	73.78 ± 20.35	71.67 ± 32.03	77.67 ± 10.18	77.00 ± 30.92	79.00 ± 27.62	74.72 ± 25.87
	CNNS + LDA-MD	89.04 ± 1.50	74.48 ± 18.41	71.93 ± 12.57	76.96± 15.51	57.78 ± 22.88	79.78 ± 14.48	85.33 ± 14.47	74.38 ± 18.79
	CNNSC + LDA-MD	89.41 ± 2.31	81.48 ± 13.41	77.04 ± 17.49	82.56 ± 14.96	64.30 ± 24.44	74.67 ± 18.14	86.22 ± 10.22	77.71 ± 18.44
	CNNS + AE	88.40 ± 1.51	86.22 ± 12.98	82.52 ± 22.39	89.59 ± 17.44	80.19 ± 18.44	82.56 ± 30.29	83.33 ± 20.99	84.07 ± 21.32
	CNNSC + AE	88.60 ± 2.26	**96.44 ± 3.98**	**96.67 ± 4.31**	**94.70 ± 6.21**	**96.22 ± 3.20**	**90.07 ± 20.10**	**91.59 ± 11.16**	**94.28 ± 10.42**

plot their ROC curves. We can notice that the proposed method (CNNSC+AE) achieves the maximum AUC value of 0.966, which is statistically larger compared with other methods ($p < 0.05$). In addition, the mean ROC curve of the proposed method is the steepest and closest to the upper left corner, indicating there is a threshold that can obtain the highest TPR while keeping the FPR very low.

To further compare the performances of these methods, Table 2 reveals the classification accuracies of different motion tasks obtained by all methods when the recall factor is set to 0.8 and 0.9, respectively. It can be noted that, although the routine method TD + LDA method achieves the highest classification accuracies (95.30%) of target motion tasks, it cannot identify any novel samples and finally misclassifies them as target motion tasks (the classification accuracies of all novel motion tasks are 0%). Other methods, however, are able to reject novel samples to varying degrees, with a sacrifice of partial ability to recognize target motion tasks, while the recall factor is used to control

this sacrifice. When the recall factor is set to 0.8; that is, the sacrifice is relatively large, we can notice that the accuracies of target motion tasks obtained by the other six methods drop to approximately 80%, while the accuracies of novel motion tasks are 88.06%, 96.26%, 92.15%, 96.83%, 99.70%, and 99.63% by the TD + LDA-MD, CNNSC + DR, CNNS + LDA-MD, CNNSC + LDA-MD, CNNS + AE, and CNNSC + AE methods, respectively. Under this condition, it is worth noting that the accuracies of novel motion tasks by the CNNS + AE and CNNSC + AE methods are almost the same ($p = 1.00$), whereas the CNNSC + LDA-MD method is significantly better than the TD + LDA-MD and CNNS + LDA-MD methods ($p < 0.05$ for each comparison). Further, when the recall factor is increased to 0.9, the classification accuracies of the six methods on the target motion tasks are correspondingly improved to about 90%, while the average accuracies of novel motion tasks by the TD + LDA-MD (77.49%), CNNSC + DR (74.72%), CNNS + LDA-MD (74.38%), CNNSC + LDA-MD (77.71%) and CNNS + AE (84.07%) methods drop sharply, except that the proposed CNNSC+AE method still achieves a satisfactory average accuracy (94.28%) and significantly outperforms other four methods ($p < 0.05$ for all comparisons).

Fig. 10 demonstrates the confusion matrices by the traditional TD + LDA-MD method and the proposed CNNSC + AE method when the recall factor is set to 0.9. In this case, we can notice that the classification accuracies of N1–N6 obtained by the CNNSC + AE method are higher than that from the TD + LDA-MD method. Besides, although misclassifications of target motion tasks (T1–T6) by the CNNSC+AE method occasionally happen, most of them are determined to be the novel pattern by mistake, which leads to no response of the control system instead of resulting in inadvertent movement during wrong identification by classifiers. However, the method of TD + LDA-MD method is more likely to output a wrong label when misclassification occurs.

Fig. 11 shows a representative example of online recognition results using the TD + LDA-MD method (Fig. 11b) and the proposed CNNSC + AE method (Fig. 11c). During identifying samples of the target motion tasks (T1–T7), these two methods have achieved similar overall performance. However, it is worth noting that all the misclassifications by the CNNSC + AE method fall into the novel class, while the TD + LDA-MD method misclassifies some samples as other target tasks. In addition, we notice that most misclassifications occur in the transient phase of each contraction. When identifying samples of novel motion tasks (N1–N6), the performance of the CNNSC + AE method is significantly better than that of the TD + LDA-MD method.

The real-time capability is crucial in myoelectric control systems. We test the running time by inputting the testing samples of one subject (2746 samples in total) into the proposed method one by one. As a result, the average processing time of one sample is 5.53±3.47 ms, which is far less than the interval between two successive samples (the increment time of data segmentation) of 150 ms, indicating that it is promising to apply our method to practical HMI systems.

5. Discussion

The ability to reject novel motion tasks is crucial in a robust myoelectric control system. This study presents a method that uses HD-sEMG and the idea of metric learning to alleviate the interference from novel motion tasks effectively.

Given the HD-sEMG, many previous studies have claimed that the spatial information derived from it can significantly improve various myoelectric control tasks [10,11,14,15,30]. Deep learning with CNN acted as the state-of-the-art spatial feature extractor, is accordingly widely adopted in the field of myoelectric control [14,26,32–34]. Generally speaking, these CNN-based approaches map the input HD-sEMG to deep features, then to the predicted labels. These studies, however, always concentrate on close-set problems, and they usually result in separable deep features to ensure superior classification performance (as evidenced in Fig. 4). It is clear in Fig. 1 that the discriminative features, rather than separable features, may be more propitious to solve the open-set problem—rejecting novel patterns. Specifically, we extract the discriminative features using a CNN trained with the idea of metric learning. Metric learning aims to learn discriminative features and is widely used in face recognition. According to the work of Wen et al. [38], we train a CNN with the softmax loss and center loss simultaneously, and use a hyperparameter λ to constrain the two losses. Fig. 5 demonstrates that the larger the λ, the smaller the intra-class distance. However, Fig. 8 tells us that although rejection performance improved with a proper λ, the curve is falling as λ increases. This can be attributed to the reason that the large λ is able to compact intra-class variations greatly, causing CNN to be insensitive to the minor differences between samples. The hyperparameter λ should be determined according to the requirements of practical application. In this study, the differences between target and novel patterns are subtle. Thus, we choose a small value of 5e−5.

Furthermore, Fig. 9 shows that the AUC value from the CNNSC + LDA-MD method is higher than that from the TD + LDA-MD and CNNS + LDA-MD methods, indicating that the discriminative deep features combined with simple rejection method can yield superior rejection performance. In addition, when another rejection method AE is adopted, the CNNSC + AE method can further improve the AUC performance and still outperform the combination of separable features (CNNS + AE). All these findings are in line with the assumption that compacting intra-class variations and enlarging inter-class differences help to reject novel samples.

Besides, consistent with previous works [39,40], we found that the performances of the CNNS + AE and CNNSC + AE methods are greater than that of any of the CNNSC + DR, CNNS + LDA-MD, and CNNSC + LDA-MD methods, indicating that the overall performance of AE is better than the traditional methods. This improvement can be attributed to the advantage of AE in mining the inherent structure of the input dataset in a nonlinear and hierarchical way. In fact, the rejection performance is also related to the recall factor assigned to the rejection method. As indicated in Table 2, we have shown that although the traditional TD + LDA method achieves high classification accuracies on target motion tasks (95.30%), they cannot reject any novel samples. The other six methods however have the ability in detecting novel samples at a cost of losing a small portion of target samples. It can be noticed that a higher recall factor always means higher classification accuracies of target motion tasks, while this may decrease the performance on novel motion tasks. The low recall factor, on the contrary, usually ensures high accuracy of identifying novel tasks and inferior performance on target tasks. This dilemma can be alleviated by adopting the proposed CNNSC + AE method, which can still achieve 94.28% classification accuracies on novel motions even if the recall factor is set to 0.9 (accuracies of novel patterns of all other methods drop sharply).

It is noteworthy that the novel motion tasks adopted in this study are more complicated than previous studies [17–25]. We predefine six novel motion tasks that can be divided into two groups: static group with isometric muscle contractions (N1–N3) and dynamic group with arbitrary contractions (N4–N6).

Consistent with previous studies [21,22], when the recall factor is set to 0.9, the TD + LDA-MD method can still accurately identify one of the static motion tasks (radial deviation in this case) with high accuracy of 89.37%, whereas the accuracies of identifying other tasks are less than 85%. This phenomenon implies that the traditional method tends to perform well in rejecting static, classifiable, novel tasks, while this ability cannot

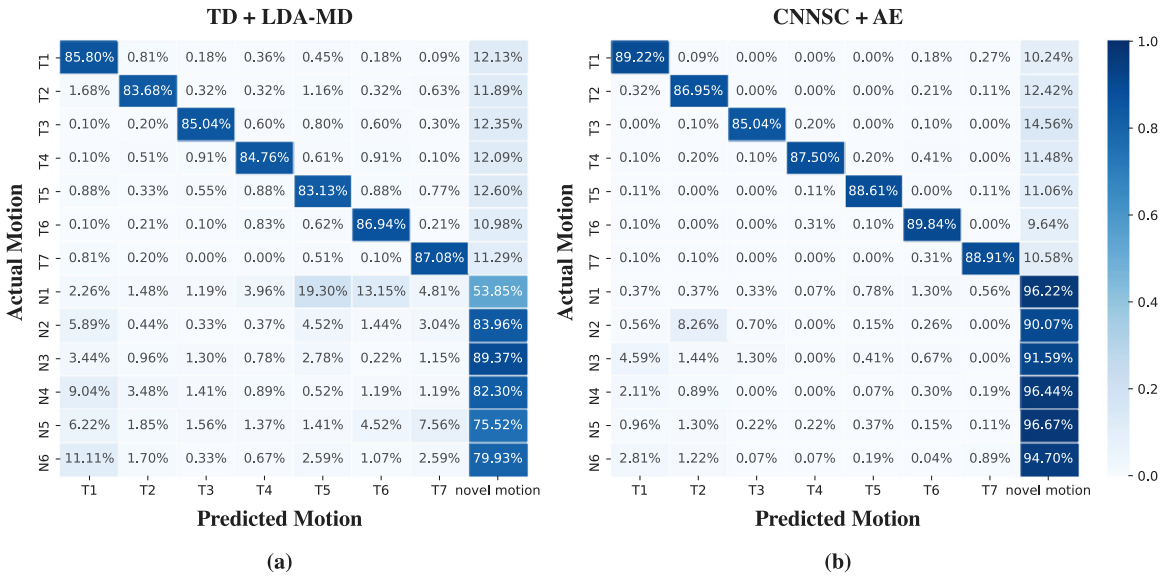

Fig. 10. Confusion matrices averaged over all subjects of the TD + LDA-MD method (a) and the proposed method (b). T1–T7 represent seven target motion tasks, while N1–N6 denote six novel motion tasks. The recall factor is set to 0.9.

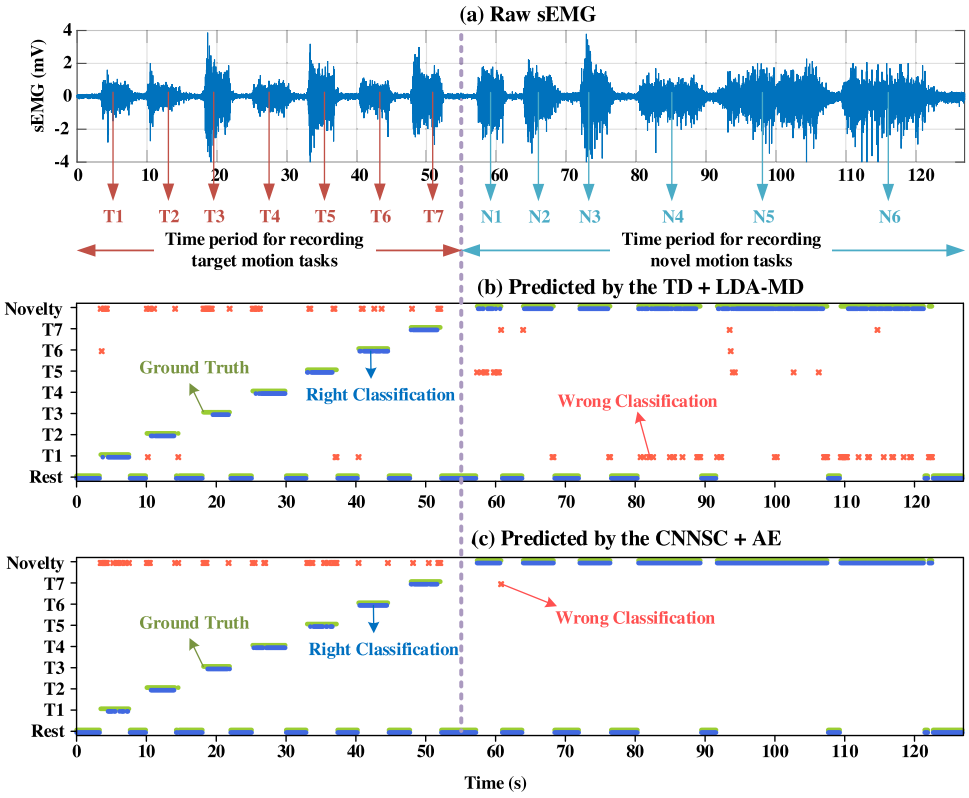

Fig. 11. Raw sEMG signals (a) of subject 1 and the recognition results predicted by TD+LDA-MD (b) and CNNSC+AE (c) methods. The recall factor is set to 0.9. In the figure, T1–T7 refer to seven target motion tasks; N1–N6 denote six novel motion tasks; the green dots are true labels; the blue dots are the correct predictions of the two methods; the red asterisks are the wrong predictions.

be generated to reject complicated novel tasks in the real scene. However, the proposed CNNSC + AE method can reject static and dynamic novel patterns with high overall accuracy of 94.28%, further reinforcing its effectiveness.

From Figs. 10 and 11, we found that most misclassifications of target samples by the proposed method are identified as novelty class, while some portion of that by the TD + LDA-MD method is recognized as other target tasks. In theory, when using a myoelectric control system, users need to spend twice as much time to correct a misclassification that prompts the device to move in the wrong direction, compared to stop the device. Furthermore, although the proposed method achieves relatively low classification accuracies on target tasks (average accuracy is 88.60% when the recall factor is set to 0.9), its active classification accuracies of the target samples (ignore target samples identified as novelty class) are approximate 100%.

Finally, we found that the proposed method outputs some unwanted novelty class during performing the target tasks, and

these misclassifications concentrate at the transient phase of the contractions. This is primarily caused by incomplete contractions due to adjustment error in the early phase and attempted compensation when stopping the contraction. Besides, intermittent rejections also happen during the contraction, which is mainly attributed to changes in samples' patterns caused by variation in force or limb orientation. Ongoing work is looking at post-processing approaches [15,45] to smooth the outputs. In addition, some latest method about novelty detection may also be exploited, such as Lee et al. [46] proposed a hierarchical classification framework to find the novel object's closest super class in the hierarchical taxonomy of known classes, and they assumed that the posterior probabilities generated by novel samples obeyed near-uniform distribution. Wu et al. [47] proposed a sequence model that uses placeholders to represent novel objects and then fill the placeholders with the help of the object detection model. Li et al. [48] facilitated vocabulary expansion and produced novel objects via a pointing mechanism. Wang et al. [49] identify if the object belongs to unseen classes using the softmax prediction and allow unseen object categories by using its semantic word embedding. These topics will be the focus of our future work.

6. Conclusion

This study proposed a myoelectric control method to alleviate the interference brought by novel motion tasks. The method first used the idea of metric learning to extract discriminative features from HD-sEMG feature images. Then multiple autoencoders were adopted for rejecting novel patterns. The proposed method achieved high accuracies on identifying complicated novel tasks, whereas the routine method failed, indicating that the proposed method is a promising method to enhance the robustness of the myoelectric pattern recognition systems.

CRediT authorship contribution statement

Le Wu: Methodology, Software, Validation, Writing - original draft. **Xu Zhang:** Conceptualization, Investigation, Visualization. **Xuan Zhang:** Validation. **Xiang Chen:** Formal analysis. **Xun Chen:** Conceptualization, Writing - review & editing, Supervision.

Declaration of competing interest

The authors declare that they have no known competing financial interests or personal relationships that could have appeared to influence the work reported in this paper.

Acknowledgment

This work was supported in part by the National Key Research and Development Program of China under Grant 2018YFB1005001 and in part by the National Natural Science Foundation of China under Grant 61922075.

References

[1] K. Englehart, B. Hudgins, A robust, real-time control scheme for multifunction myoelectric control, IEEE Trans. Biomed. Eng. 50 (2003) 848–854.
[2] P. Delatorre, C. Leon, A.G. Salguero, A. Tapscott, Predicting the effects of suspenseful outcome for automatic storytelling, Knowl.-Based Syst. 209 (2020) 106450.
[3] Z.Z. Bien, H.-E. Lee, Effective learning system techniques for human–robot interaction in service environment, Knowl.-Based Syst. 20 (2007) 439–456.
[4] Y. Huang, K.B. Englehart, B. Hudgins, A.D. Chan, A Gaussian mixture model based classification scheme for myoelectric control of powered upper limb prostheses, IEEE Trans. Biomed. Eng. 52 (2005) 1801–1811.
[5] P. Parker, K. Englehart, B. Hudgins, Myoelectric signal processing for control of powered limb prostheses, J. Electromyography Kinesiol. 16 (2006) 541–548.
[6] H.S. Lo, S.Q. Xie, Exoskeleton robots for upper-limb rehabilitation: State of the art and future prospects, Med. Eng. Phys. 34 (2012) 261–268.
[7] R. Gopura, D. Bandara, K. Kiguchi, G.K. Mann, Developments in hardware systems of active upper-limb exoskeleton robots: A review, Robot. Auton. Syst. 75 (2016) 203–220.
[8] J. Nishida, K. Suzuki, A paired wearable device for blending kinesthetic experience, in: Proceedings of the 2017 CHI Conference on Human Factors in Computing Systems, 2017, pp. 3316-3327.
[9] S.-w. Leigh, P. Maes, Body integrated programmable joints interface, in: Proceedings of the 2016 CHI Conference on Human Factors in Computing Systems, 2016, pp. 6053-6057.
[10] X. Zhang, P. Zhou, High-density myoelectric pattern recognition toward improved stroke rehabilitation, IEEE Trans. Biomed. Eng. 59 (2012) 1649–1657.
[11] S. Zhang, X. Zhang, S. Cao, X. Gao, X. Chen, P. Zhou, Myoelectric pattern recognition based on muscle synergies for simultaneous control of dexterous finger movements, IEEE Trans. Hum.-Mach. Syst. 47 (2017) 576–582.
[12] J. Cheng, F. Wei, C. Li, Y. Liu, A. Liu, X. Chen, Position-independent gesture recognition using sEMG signals via canonical correlation analysis, Comput. Biol. Med. 103 (2018) 44–54.
[13] X. Chen, Z.J. Wang, Pattern recognition of number gestures based on a wireless surface EMG system, Biomed. Signal Process. Control 8 (2013) 184–192.
[14] X. Zhang, L. Wu, B. Yu, X. Chen, X. Chen, Adaptive calibration of electrode array shifts enables robust myoelectric control, IEEE Trans. Biomed. Eng. 67 (2020) 1947–1957.
[15] B. Yu, X. Zhang, L. Wu, X. Chen, X. Chen, A novel postprocessing method for robust myoelectric pattern-recognition control through movement pattern transition detection, IEEE Trans. Hum.-Mach. Syst. 50 (2020) 32–41.
[16] B. Hudgins, P. Parker, R.N. Scott, A new strategy for multifunction myoelectric control, IEEE Trans. Biomed. Eng. 40 (1993) 82–94.
[17] E.J. Scheme, K.B. Englehart, B.S. Hudgins, Selective classification for improved robustness of myoelectric control under nonideal conditions, IEEE Trans. Biomed. Eng. 58 (2011) 1698–1705.
[18] Q. Ding, X. Zhao, J. Han, C. Bu, C. Wu, Adaptive hybrid classifier for myoelectric pattern recognition against the interferences of outlier motion, muscle fatigue, and electrode doffing, IEEE Trans. Neural Syst. Rehabil. Eng. 27 (2019) 1071–1080.
[19] Y.-H. Liu, H.-P. Huang, Towards a high-stability EMG recognition system for prosthesis control: A one-class classification based non-target EMG pattern filtering scheme, in: 2009 IEEE International Conference on Systems, Man and Cybernetics, IEEE, 2009, pp. 4752–4757.
[20] E.J. Scheme, K.B. Englehart, Validation of a selective ensemble-based classification scheme for myoelectric control using a three-dimensional Fitts' law test, IEEE Trans. Neural Syst. Rehabil. Eng. 21 (2012) 616–623.
[21] S. Amsuess, I. Vujaklija, P. Goebel, A.D. Roche, B. Graimann, O.C. Aszmann, D. Farina, Context-dependent upper limb prosthesis control for natural and robust use, IEEE Trans. Neural Syst. Rehabil. Eng. 24 (2015) 744–753.
[22] Q. Ding, Z. Li, X. Zhao, Y. Xiao, J. Han, Real-time myoelectric prosthetic-hand control to reject outlier motion interference using one-class classifier, in: 2017 32nd Youth Academic Annual Conference of Chinese Association of Automation (YAC), IEEE, 2017, pp. 96–101.
[23] E.J. Scheme, B.S. Hudgins, K.B. Englehart, Confidence-based rejection for improved pattern recognition myoelectric control, IEEE Trans. Biomed. Eng. 60 (2013) 1563–1570.
[24] J.W. Robertson, K.B. Englehart, E.J. Scheme, Effects of confidence-based rejection on usability and error in pattern recognition-based myoelectric control, IEEE J. Biomed. Health Inf. 23 (2018) 2002–2008.
[25] J. Tomczyński, P. Kaczmarek, T. Mańkowski, Hand gesture-based interface with multichannel sEMG band enabling unknown gesture discrimination, in: 2015 10th International Workshop on Robot Motion and Control (RoMoCo), IEEE, 2015, pp. 52–57.
[26] A. Ameri, M.A. Akhaee, E. Scheme, K. Englehart, A deep transfer learning approach to reducing the effect of electrode shift in EMG pattern recognition-based control, IEEE Trans. Neural Syst. Rehabil. Eng. 28 (2019) 370–379.
[27] L. Wu, X. Zhang, K. Wang, X. Chen, X. Chen, Improved high-density myoelectric pattern recognition control against electrode shift using data augmentation and dilated convolutional neural network, IEEE Trans. Neural Syst. Rehabil. Eng. (2020) 1.
[28] A.H. Al-Timemy, R.N. Khushaba, G. Bugmann, J. Escudero, Improving the performance against force variation of EMG controlled multifunctional upper-limb prostheses for transradial amputees, IEEE Trans. Neural Syst. Rehabil. Eng. 24 (2015) 650–661.

[29] R.N. Khushaba, A.H. Al-Timemy, A. Al-Ani, A. Al-Jumaily, A framework of temporal-spatial descriptors-based feature extraction for improved myoelectric pattern recognition, IEEE Trans. Neural Syst. Rehabil. Eng. 25 (2017) 1821–1831.
[30] D. Wang, X. Zhang, X. Gao, X. Chen, P. Zhou, Wavelet packet feature assessment for high-density myoelectric pattern recognition and channel selection toward stroke rehabilitation, Front. Neurol. 7 (2016) 197.
[31] F. Schroff, D. Kalenichenko, J. Philbin, Facenet: A unified embedding for face recognition and clustering, in: Proceedings of the IEEE conference on computer vision and pattern recognition, 2015, pp. 815-823.
[32] G. Zhu, X. Zhang, X. Tang, X. Chen, X. Gao, Examining and monitoring paretic muscle changes during stroke rehabilitation using surface electromyography: A pilot study, Math. Biosci. Eng. 17 (2020) 216–234.
[33] L. Wu, X. Zhang, X. Chen, X. Chen, Visualized evidences for detecting novelty in myoelectric pattern recognition using 3D convolutional neural networks, in: 2019 41st Annual International Conference of the IEEE Engineering in Medicine and Biology Society (EMBC), IEEE, 2019, pp. 2641–2644.
[34] W. Wei, Q. Dai, Y. Wong, Y. Hu, M. Kankanhalli, W. Geng, Surface-electromyography-based gesture recognition by multi-view deep learning, IEEE Trans. Biomed. Eng. 66 (2019) 2964–2973.
[35] A.T. Nguyen, J. Xu, M. Jiang, D.K. Luu, T. Wu, W.-k. Tam, W. Zhao, M.W. Drealan, C.K. Overstreet, Q. Zhao, A bioelectric neural interface towards intuitive prosthetic control for amputees, J. Neural Eng. 17 (2020) 066001.
[36] P. Tsinganos, B. Cornelis, J. Cornelis, B. Jansen, A. Skodras, Hilbert sEMG data scanning for hand gesture recognition based on deep learning, Neural Comput. Appl. (2020) 1–22.
[37] D. Xiong, D. Zhang, X. Zhao, Y. Zhao, Deep learning for EMG-based human-machine interaction: A review, IEEE/CAA J. Autom. Sinica 8 (2021) 512–533.
[38] Y. Wen, K. Zhang, Z. Li, Y. Qiao, A discriminative feature learning approach for deep face recognition, in: European Conference on Computer Vision, Springer, 2016, pp. 499–515.
[39] M. Sakurada, T. Yairi, Anomaly detection using autoencoders with nonlinear dimensionality reduction, in: Proceedings of the MLSDA 2014 2nd Workshop on Machine Learning for Sensory Data Analysis, 2014, pp. 4-11.
[40] K.H. Kim, S. Shim, Y. Lim, J. Jeon, J. Choi, B. Kim, A.S. Yoon, Rapp: Novelty detection with reconstruction along projection pathway, Int. Conf. Learn. Represent. (2019).
[41] L.v.d. Maaten, G. Hinton, Visualizing data using t-SNE, J. Mach. Learn. Res. 9 (2008) 2579–2605.
[42] M.D. Zeiler, Adadelta: an adaptive learning rate method, 2012, arXiv preprint arXiv:1212.5701.
[43] J.R. Bray, J.T. Curtis, An ordination of the upland forest communities of southern wisconsin, Ecol. Monograph 27 (1957) 326–349.
[44] J.A. Hanley, B.J. McNeil, The meaning and use of the area under a receiver operating characteristic (ROC) curve, Radiology 143 (1982) 29–36.
[45] T.-E. Lin, H. Xu, A post-processing method for detecting unknown intent of dialogue system via pre-trained deep neural network classifier, Knowl.-Based Syst. 186 (2019) 104979.
[46] K. Lee, K. Lee, K. Min, Y. Zhang, J. Shin, H. Lee, Hierarchical novelty detection for visual object recognition, in: Proceedings of the IEEE Conference on Computer Vision and Pattern Recognition, 2018, pp. 1034-1042.
[47] Y. Wu, L. Zhu, L. Jiang, Y. Yang, Decoupled novel object captioner, in: Proceedings of the 26th ACM international conference on Multimedia, 2018, pp. 1029-1037.
[48] Y. Li, T. Yao, Y. Pan, H. Chao, T. Mei, Pointing novel objects in image captioning, in: Proceedings of the IEEE/CVF Conference on Computer Vision and Pattern Recognition, 2019, pp. 12497-12506.
[49] S. Wang, K.-H. Yap, J. Yuan, Y.-P. Tan, Discovering human interactions with novel objects via zero-shot learning, in: Proceedings of the IEEE/CVF Conference on Computer Vision and Pattern Recognition, 2020, pp. 11652-11661.